frontiers in Earth Science

ORIGINAL RESEARCH
published: 28 March 2022
doi: 10.3389/feart.2022.799280

Paleoclimate Records of the Middle Okinawa Trough Since the Middle Holocene: Modulation of the Low-Latitude Climate

Lei Liu[1,2,3,4], *Hongxiang Guan*[1,2,3]*, *Lanfang Xu*[5,6], *Zhilei Sun*[3,4] *and Nengyou Wu*[1,3,4]*

[1]*Frontiers Science Center for Deep Ocean Multispheres and Earth System, Department of Environment Science and Engineering, Ocean University of China, Qingdao, China,* [2]*Key Lab of Submarine Geosciences and Prospecting Techniques, MOE and College of Marine Geosciences, Ocean University of China, Qingdao, China,* [3]*Laboratory for Marine Mineral Resources, Qingdao National Laboratory for Marine Science and Technology, Qingdao, China,* [4]*Key Laboratory of Gas Hydrate, Qingdao Institute of Marine Geology, Ministry of Natural Resources, Qingdao, China,* [5]*Guangzhou Institute of Energy Conversion, Chinese Academy of Sciences, Guangzhou, China,* [6]*University of Chinese Academy of Sciences, Beijing, China*

The ubiquity of glycerol dibiphytanyl glycerol tetraethers (GDGTs) and their temperature sensitivity make them one of the most effective tools for paleoclimate reconstruction. High- and low-latitude climates influence the Okinawa Trough (OT). It receives diverse inputs from the East China Sea, the western Pacific, and the Kuroshio Current, providing good conditions for paleoclimate studies. Here, isoprenoid GDGTs (isoGDGTs), branched GDGTs, and hydroxylated GDGTs (OH-GDGTs) were studied to reconstruct the sea surface temperature (SST) of the central OT for the past 8.2 kyr using the tetraether index of 86 carbon atoms at low latitudes (TEX_{86}^{H}) and the ring index of OH-GDGTs (RI-OH). The GDGT-0/crenarchaeol ratios ranged from 0.39 to 0.98. The branched and isoprenoid tetraether index and the methane index values were lower than 0.1 and 0.5, respectively, indicating that the isoGDGTs were mainly derived from marine *Thaumarchaeota* and that TEX_{86}^{H} could be used to reconstruct the paleotemperatures. The TEX_{86}^{H} SSTs ranged from 21.6 to 27.2°C during 8.2 kyr. The overall range of TEX_{86}^{H} SSTs is close to the $U_{37}^{K'}$ SST of the middle OT and reflects the mean annual SST. In contrast, RI-OH temperatures varied from 17.4 to 26.0°C, showing a lower trend than TEX_{86}^{H} SSTs. The core top RI-OH temperature is 24.1°C, in line with the mean annual seawater temperature at 40 m (24.2°C) in the study area, which likely reflects the subsurface temperature in this case. The small overall warming trend of TEX_{86}^{H} SSTs agrees with the increasing intensity of the Kuroshio Current during the last 8.2 kyr, indicating that the SST evolution is governed by the Kuroshio Current that transports heat from the western tropical Pacific. The decreasing temperature differences between TEX_{86}^{H} and RI-OH and between $U_{37}^{K'}$ and RI-OH showed increased mixing of the upper water column, which was in good accordance with the increasing low-latitude winter insolation decoupling from the East Asian summer monsoon. The cold event that occurred at 7.4–6.6 kyr was magnified (~5°C) at the TEX_{86}^{H} and RI-OH temperatures and possibly caused by tephra's significant input (~7.3 kyr).

Keywords: isoprenoid glycerol dibiphytanyl glycerol tetraethers, hydroxylated glycerol dibiphytanyl glycerol tetraethers, TEX_{86}^{H}, sea surface temperature, okinawa trough

OPEN ACCESS

Edited by:
Jiangong Wei,
Guangzhou Marine Geological Survey, China

Reviewed by:
Xiaowei Zhu,
South China Sea Institute of Oceanology, CAS, China
Zhifeng Wan,
Sun Yat-sen University, China

****Correspondence:***
Hongxiang Guan
guanhongxiang@ouc.edu.cn
Nengyou Wu
wuny@ms.giec.ac.cn

Specialty section:
This article was submitted to Geochemistry, a section of the journal Frontiers in Earth Science

Received: *21 October 2021*
Accepted: *18 February 2022*
Published: *28 March 2022*

Citation:
Liu L, Guan H, Xu L, Sun Z and Wu N (2022) Paleoclimate Records of the Middle Okinawa Trough Since the Middle Holocene: Modulation of the Low-Latitude Climate. Front. Earth Sci. 10:799280. doi: 10.3389/feart.2022.799280

INTRODUCTION

The Okinawa Trough, located in the western North Pacific, was influenced by the East Asian monsoon (ESM). Paleoclimate records indicated that correlations between temperature variation and East Asian summer monsoon (EASM) precipitation have become weak since the middle Holocene (Liew et al., 2006; Peterse et al., 2011; Park et al., 2014). However, such records in marine sediments are sparse (Xu et al., 2018 and references therein). The Okinawa Trough (OT) has been regarded as an ideal location for paleoclimatic, paleohydrogeological, and paleoceanographic studies because it is within the influence of the climate of both the high-latitude North Atlantic and the low-latitude western Pacific Ocean (Sun et al., 2005; Kubota et al., 2010; Ruan et al., 2015; Xu et al., 2018). The seasonal variations in EAM are driven by Northern Hemisphere summer and winter solar insolation, reflecting teleconnection with the high-latitude North Atlantic (An et al., 2001; Wang et al., 2005; Ruan et al., 2015; Huang and Sarnthein, 2021). The Kuroshio Current (KC) originates from the western Pacific warm pool and transports massive amounts of warm and salty water into the OT (Hu et al., 2015; Zheng et al., 2016). Paleoclimate indicators have demonstrated the influences of both the EAM and KC on the OT paleoclimate, such as oxygen isotopes (Kubota et al., 2010), Mg/Ca ratios of planktonic foraminifera (Sun et al., 2005), alkenone unsaturation index ($U^{K'}_{37}$; Ruan et al., 2015), and the tetraether index of 86 carbon atoms (TEX_{86}; Xu et al., 2018). Sea surface temperatures (SSTs) from different locations of the OT tend to reveal different controlling factors on the paleoclimate (Ruan et al., 2015; Zhao et al., 2015; Xu et al., 2018). The cold anomalies recorded in the northern Atlantic, such as the 4 kyr event, have affected the northern and southern OT paleoclimate (Sun et al., 2005; Ruan et al., 2015; Zhao et al., 2015). The $U^{K'}_{37}$ SST of the southern OT has been observed to have decreased since 7.4 kyr BP (Ruan et al., 2015), which was attributed to the reduction in Northern Hemisphere summer solar insolation and the weakening of EASM intensity (Ruan et al., 2015 and references therein). However, in the southern OT, Xu et al. (2018) found that paleotemperatures from $U^{K'}_{37}$/TEX_{86} decoupled from the EASM during the last 13.3 kyr BP. In contrast, the western tropical Pacific and Northern Hemisphere winter solar insolation were demonstrated to be the controlling factors of SSTs. Whether EAM changes in the OT are in phase with temperature changes in the EAM region during the Holocene remains unsolved (Liew et al., 2006; Peterse et al., 2011; Park et al., 2014). Therefore, further investigations are needed to elucidate the OT paleotemperature evolution and the controlling factors.

The TEX_{86} index (**Table 1**) was proposed by Schouten et al. (2002) based on the increasing number of cyclopentane rings in isoprenoid glycerol dibiphytanyl glycerol tetraethers (isoGDGTs) with increasing temperature (Gliozzi et al., 1983; Uda et al., 2001; Sinninghe Damsté et al., 2002). The export depth of the TEX_{86} signal in the water column is still under debate (Schouten et al., 2002, 2013; Ingalls et al., 2006; Rueda et al., 2009; Jia et al., 2012; Zhang and Liu, 2018). Most researchers now regard TEX_{86} as a better reflection of subsurface temperatures (Huguet et al., 2007; Jia et al., 2012). However, some studies have shown that TEX_{86} corresponds well with the annual mean SST (Ingalls et al., 2006; Rueda et al., 2009). Consequently, the use of TEX_{86} for temperature reconstruction in specific areas needs to be evaluated.

Marine Group I (MG-I) *Thaumarchaeota* were proposed to produce isoGDGTs used in the TEX_{86} equation (**Table 1**; **Supplementary Figure S1**; Brochier-Armanet et al., 2008; Spang et al., 2010). To achieve better accuracy, Kim et al. (2010) proposed TEX^{L}_{86} for high latitudes (<15°C) and TEX^{H}_{86} for low latitudes (>15°C) according to studies on global ocean samples (**Table 1**). To further assess the proxy, the Bayesian regression approach, which offers several advantages, was introduced to the TEX_{86}–SST calibration to provide a comprehensive estimation of past changes in SST from TEX_{86} in both modern and ancient environments (Tierney and Tingley, 2014). However, many environmental factors, except for SSTs, are included in the Bayesian regression approach for TEX_{86}–SST calibrations, making it more challenging to apply in geological sites than TEX^{L}_{86}/TEX^{H}_{86} (Kim et al., 2010; Tierney and Tingley, 2014). Since isoprenoid tetraethers produced by marine *Thaumarchaeota* can be mixed with those from *Euryarchaeota* thriving in seawater and *Thaumarchaeota* in soils, indicators such as branched and isoprenoid tetraether index (BIT; Hopmans et al., 2004) and methane index (MI; Zhang et al., 2011) are used to assess isoGDGTs contributed from soil origin and *Euryarchaeota*. For example, an MI less than 0.5 is used to preclude the contribution of methanotrophic archaea (Zhang et al., 2011). In addition to isoGDGTs, hydroxylated GDGTs (OH-GDGTs) are widespread in marine environments (Liu et al., 2012; Fietz et al., 2013; Huguet et al., 2013; Lü et al., 2015). In culture experiments, archaea affiliated with *Thaumarchaeota* Group I.1a have produced OH-GDGTs (Liu et al., 2012; Elling et al., 2014), which were not observed in *Thaumarchaeota* Group I.1b (Sinninghe Damsté et al., 2012b). The ratio of sum OH-GDGTs relative to sum isoGDGTs was related to SSTs and increased with increasing latitude (Huguet et al., 2013). In addition, a positive correlation between the number of cyclopentane rings of OH-GDGTs and SSTs was reported in the surface sediments from the subpolar and polar areas (Fietz et al., 2013). Although the mechanism for OH-GDGTs in response to SST is unclear, the ring index based on OH-GDGTs (RI-OH) is a potential approach for temperature reconstruction (**Table 1**; Lü et al., 2015; Yang et al., 2018).

TABLE 1 | Initial definitions of various proxies are used in this article.

Index	Definitions	authors
TEX_{86}	$(\frac{GDGT-2+GDGT-3+crenarchaeol\ isomer}{GDGT-1+GDGT-2+GDGT-3+crenarchaeol\ isomer})$	Schouten et al. (2002)
TEX^{L}_{86}	$log(\frac{GDGT-2}{GDGT-1+GDGT-2+GDGT-3})$	Kim et al. (2010)
RI − OH	$\frac{[OH-GDGT-1]+2\times[OH-GDGT-2]}{[OH-GDGT-1]+[OH-GDGT-2]}$	Lü et al. (2015)
BIT	$\frac{([GDGT-Ia]+[GDGT-IIa]+[GDGT-IIIa])}{([GDGT-Ia]+[GDGT-IIa]+[GDGT-IIIa]+Crenarchaeol)}$	Hopmans et al. (2004)
MI	$\frac{[GDGT-1]+[GDGT-2]+[GDGT-3]}{[GDGT-1]+[GDGT-2]+[GDGT-3]+[Crenarchaeol]+[crenarchaeol\ isomer]}$	Zhang et al. (2011)
%GDGT − 2	$\frac{GDGT-2}{[GDGT-1]+[GDGT-2]+[GDGT-3]+[crenarchaeol\ isomer]}$	Sinninghe Damsté et al. (2012a)

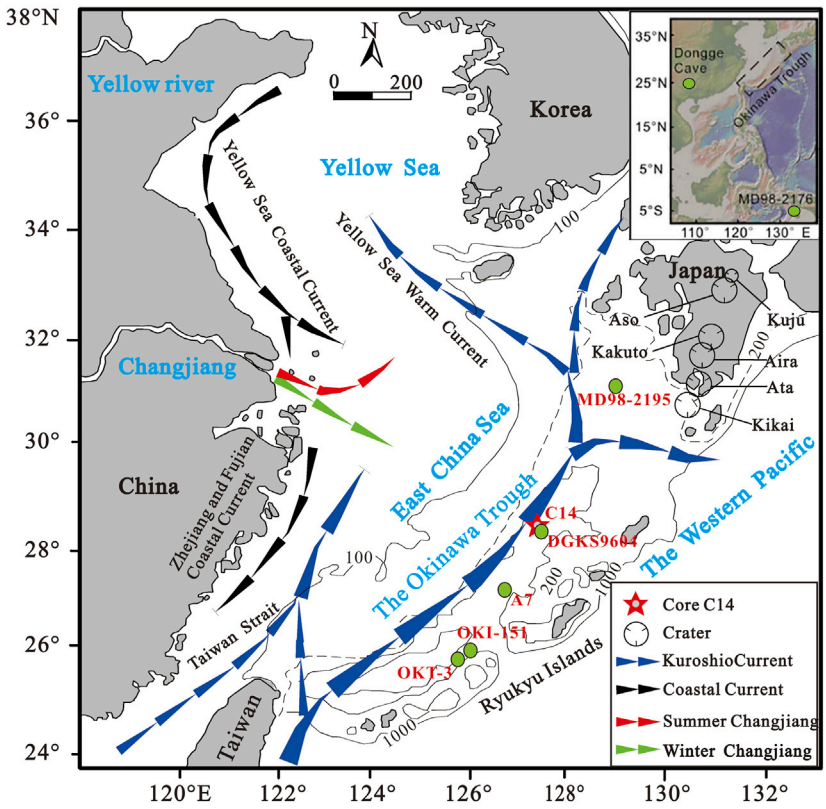

FIGURE 1 | Location of core C14 in the middle Okinawa Trough (OT) and selected paleoenvironmental settings, including Dongge Cave in southern China (Dykoski et al., 2005), core MD98-2176 in the western tropical Pacific (Stott et al., 2004), cores A7 (Sun et al., 2005) and DGKS9604 (Yu et al., 2009) in the middle OT, cores OKT-3 (Zhao et al., 2015) and OKI-151 (Xu et al., 2018) in the southern OT, and core MD98-2195 (Yamamoto et al., 2013) in the northern OT. The map was revised from Dou et al. (2010). The Contour unit is meter. Volcano locations around Japan were modified according to Machida (1999).

TEX_{86}^{H} has been used to reconstruct the paleotemperature records of the southern and northern OT, and a gradual warming trend has been identified since the Holocene (Yamamoto et al., 2013; Zhao et al., 2015; Xu et al., 2018). Generally, shifts in the main axis and changes in the KC strength, variations in EAM, sea-level changes, and freshwater inputs are potential factors for paleoclimate changes in the OT (Jian et al., 2000; Kubota et al., 2010; Zhao et al., 2015). The influence of the EAM on SST variations was identified in the middle and northern OT (Yu et al., 2009; Kubota et al., 2010). However, low-latitude western tropical Pacific dominance via KC variations has been demonstrated in the southern OT (Xu et al., 2018). Therefore, factors controlling the paleotemperature in specific areas of the OT need to be clarified. Here, we used TEX_{86}^{H} temperatures and temperatures calibrated from RI-OH as an approach to reconstruct the paleoclimate and hydrological evolution of the middle OT since the middle Holocene.

OCEANOGRAPHIC SETTING

The OT, a back-arc basin, formed from the subduction of the Philippine Sea Plate beneath the Eurasian Plate at the Ryukyu Trench (**Figure 1**; Sibuet et al., 1998; Guo et al., 2022). The strike direction of the middle OT is approximately NE–SW, E–W to the south, and NNE–SSW to the north (Wu et al., 2014). The EAM and KC have been reported to dominate the modern oceanography of the middle OT (Ruan et al., 2015; Zhao et al., 2015). Two distinct seasons are present due to the seasonal reversals of the EAM, driven by the annual cycle of insolation and its effect on the land-sea thermal contrast (Dykoski et al., 2005; Sun et al., 2005; Wang et al., 2005; Huang and Sarnthein, 2021). In the boreal summer, a warm, wet season caused by the northward migration of the intertropical convergence zone and the maximum monsoonal convective rainfall dominates the OT (Wang et al., 2005; Zheng et al., 2014). In contrast, northeasterly winds lead to a cool, dry season in the boreal winter (Diekmann et al., 2008; Zheng et al., 2014). The KC, originating from the Western Pacific warm pool, flows northeast above the OT and returns to the North Pacific through the Tokara Strait (Yu et al., 2009; Hu et al., 2015), taking warm, saline water into the OT (Hu et al., 2015).

The sea level has been roughly constant for the study area during the last 8.2 kyr BP (Liu et al., 2004). The sediment core C14 is far from the coastline and the shelf of the East China Sea (ECS; **Figure 1**). At present, the mean annual SST is 24.8°C, with

TABLE 2 | Planktonic foraminifera ^{14}C age data.

series	Depth (cmbsf)	Planktonic foraminifera	AMS ^{14}C age (yr BP)	Calibrated age (yr BP)
498910	35–37.5[a]	*G.ruber* + *G.sacculifer*	660±30	616–730
498911	65–67.5	*G.ruber* + *G.sacculifer*	930±30	994–820
498912	155–157.5[a]	*G.ruber* + *G.sacculifer*	1890±30	1858–2045
498913	245–247.5	*G.ruber* + *G.sacculifer*	2800±30	3172–2957
498914	365–367.5[a]	*G.ruber* + *G.sacculifer*	4350±30	4943–5227
498915	455–457.5	*G.ruber* + *G.sacculifer*	5840±30	6831–6646
498916	545–547.5	*G.ruber* + *G.sacculifer*	6500±30	7520–7385
498917	575–577.5[a]	*G.ruber* + *G.sacculifer*	7340±30	8170–8327

[a]*Data from Xu et al. (2020).*

summer and winter seasonal temperatures of approximately 27.8 and 22.1°C, respectively. The maximum SST near the core site is 28.7 °C in August, and the minimum is 21.5°C in February (Locarnini et al., 2013).

METHODS

Materials and Age Model

Sediment core C14 (580 cm in length) was retrieved from the middle OT at a water depth of approximately 1100 m (**Figure 1**; 28°39.587′N, 127°19.194′E). The top part of the core was lost during sampling. To make up the lost part, the upper 10 cm of core C10 (28°38.8′N, 127°21.283′E; water depth of 960 m) was utilized to represent the missing top part. After sampling, the sediment core was segmented, transported to the laboratory, and kept at −20°C until analysis. A tephra layer was found between depths of 532.5 and 442.5 cm.

To obtain AMS ^{14}C dating for the core, eight samples of the planktonic foraminifer *Globigerinoides ruber* (*G. ruber*) and *G. sacculifer* were selected at equal intervals and analyzed by Beta Analytic Inc., United States (**Table 2**). The raw ^{14}C dates were calibrated using the Marine13 dataset (Reimer et al., 2013) and expressed in calibrated years BP (years before AD 1950). We adopted a ΔR value of 30 ± 41 years in the calibration.

Lipid Extraction

37 samples were collected at 15–30 cm intervals from core C14 (36 samples from core C14 and 1 from core C10). They were freeze-dried and homogenized. Twenty to 30 g of powder (dry weight) were Soxhlet-extracted for 72 h with a mixture of dichloromethane and methanol (9:1; v:v) to obtain the total lipid extracts (TLEs). The TLE was separated into neutral (n-hexane) and polar (methanol) fractions with a silica gel column. The polar fractions were filtered through a 0.45 μm polytetrafluoroethylene filter membrane (PTFE) to remove particulate matter and stored at −20°C.

Instrumental Analysis

The dried polar fractions were redissolved in 300 μl *n*-hexane and isopropanol (98.2:1.8, v/v). No internal standard was added. The analysis was performed on an Agilent 1200 series high-performance liquid chromatography–atmospheric pressure chemical ionization-6460 triple, quadruple mass spectrometer (HPLC–APCI-MS^2) following the analytical protocol of Hopmans et al. (2016). Separation was achieved on two HPLC silica columns (BEH HILIC columns, 2.1 × 150 mm, 1.7 μm) in series, maintained at 30°C. The GDGTs were eluted isocratically for 25 min with 18% B, followed by a linear gradient to 35% B in 25 min and then a linear gradient to 100% B in 30 min and kept in for 10 min to clean the column with a constant flow rate of 0.2 ml/min. Finally, the gradient of B was back at 18% for 20 min to re-equilibrate the column. Solvent A was *n*-hexane, and B was *n*-hexane: isopropanol (9:1, v/v). The GDGTs were ionized in an atmospheric pressure chemical ionization chamber and detected using single ion monitoring (SIM) mode. The relative abundance of compounds was determined by integrating the areas of the $(M + H]^+$ (protonated molecular ion) peaks at 1302, 1300, 1298, 1296, and 1292 for isoGDGTs and OH-GDGTs (Liu et al., 2012) and 1050, 1048, 1046, 1036, 1034, 1032, 1022, 1020, and 1018 for branched GDGTs (brGDGTs). The analytical error for duplicate measurements was better than ±0.008. The positive ion APCI settings were set as follows (Hopmans et al., 2016): probe heater temperature, 400°C; sheath gas (N_2) pressure, 50 AU (arbitrary units); auxiliary gas (N_2) pressure, 5 AU; spray current, 5 μ A; capillary temperature, 3500°C; S-lens, 100 V.

TEX_{86}^{H}, RI-OH and BIT

In this study, the SST calibration of the TEX_{86}^{H} proxy (Kim et al., 2010) was used to reconstruct the paleoclimate evolution due to the high temperatures of over 15°C (low latitude) in the OT. Cren' represents the crenarchaeol isomer (see **Supplementary Figure S1** for details).

$$TEX_{86}^{H} = \log\left(\frac{GDGT-2+GDGT-3+Cren'}{GDGT-1+GDGT-2+GDGT-3+Cren'}\right);$$
$$SST = 68.4 \times \left(TEX_{86}^{H}\right) + 38.6 \quad (1)$$

The empirical equation of RI-OH (Lü et al., 2015) was used to supplement the SST reconstruction.

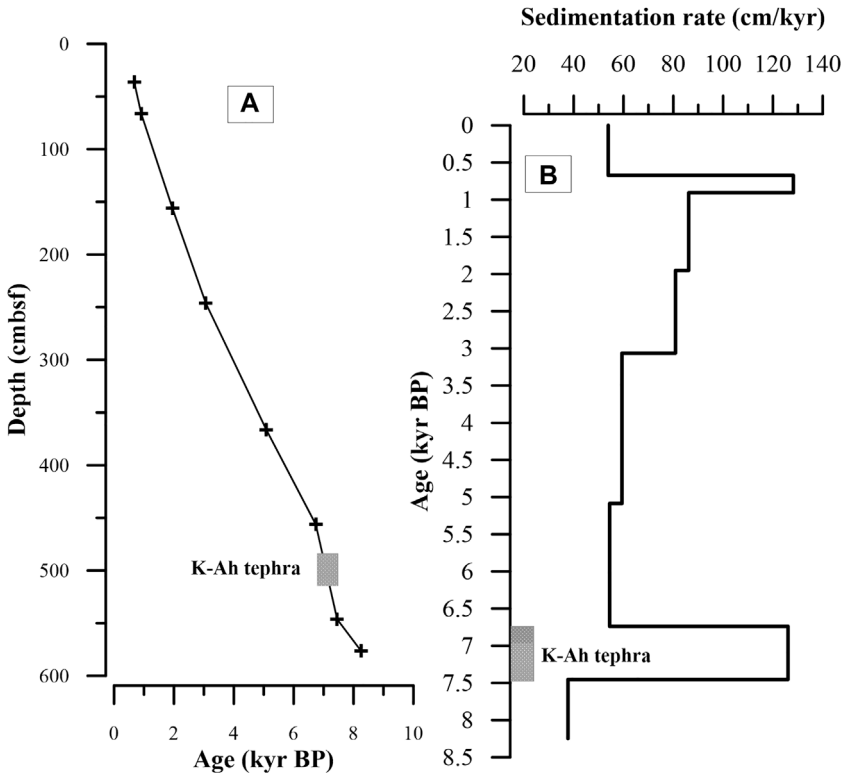

FIGURE 2 | (A) Age-depth model of core C14; **(B)** sedimentation rates of core C14.

$$\begin{aligned} \text{RI}-\text{OH} &= \frac{[\text{OH}-\text{GDGT}-1]+2\times[\text{OH}-\text{GDGT}-2]}{[\text{OH}-\text{GDGT}-1]+[\text{OH}-\text{GDGT}-2]}; \\ \text{SST} &= 35.71\times\text{RI}-\text{OH}-32.86 \end{aligned} \tag{2}$$

Based on the analytical error (±0.008), we calculated the corresponding errors, which are approximately ±0.4°C and ±0.3°C for calibrations 1) and (2), respectively.

As brGDGT regio isomers were detected (**Supplementary Figure S1**; De Jonge et al., 2014), the BIT formula used in this article was modified as follows:

$$\text{BIT} = \frac{\begin{array}{c}\text{GDGT}-\text{Ia}+\text{GDGT}-\text{IIa}+\text{GDGT}-\text{IIa}' \\ +\text{GDGT}-\text{IIIa}+\text{GDGT}-\text{IIIa}'\end{array}}{\begin{array}{c}\text{Crenarcheaol}+\text{GDGT}-\text{Ia}+\text{GDGT}-\text{IIa} \\ +\text{GDGT}-\text{IIa}'+\text{GDGT}-\text{IIIa}+\text{GDGT}-\text{IIIa}'\end{array}} \tag{3}$$

RESULTS

AMS ^{14}C Dating

The AMS ^{14}C dating results are listed in **Table 2**. The time scale was established by linear interpolation and extrapolation. An age model was set for core C14 after calibration, and the mean sedimentation rate of core C14 was ~70 cm/kyr during the last 8.2 kyr BP (**Figures 2A,B**). For the tephra layer at 532.5–442.5 cm (7.4–6.6 kyr BP), an extremely high sedimentation rate of ~126 cm/kyr was identified (**Figure 2B**).

Distribution of GDGTs

The relative contributions of the isoGDGTs, brGDGTs, and OH-GDGTs are listed in **Table 3**. The isoGDGTs dominated all GDGTs, with contributions ranging from 88 to 98%, while brGDGTs accounted for 1.4–10.3%, and OH-GDGTs accounted for less than 6.0% of the total GDGTs. Crenarchaeol was the most abundant component among the isoGDGTs in all of the samples, accounting for 32–50% of all of the isoGDGTs, followed by GDGT-0 (range 16–32%), whereas only small amounts of GDGT-1, -2, -3, and the crenarchaeol isomer were detected in all of the samples.

Past Temperatures Reconstructed by isoGDGT- and OH-GDGT-Based Proxies

For the past 8.2 kyr BP, the $\text{TEX}_{86}^{\text{H}}$ values in core C14 ranged from −0.25 to −0.17, corresponding to temperatures ranging from 21.6 to 27.2°C (**Equation 2**; **Table 4**; **Figure 3C**). The index of RI-OH in core C14 ranged from 1.41 to 1.65, revealing temperatures ranging from 17.4 to 26.0°C (**Equation 3**; **Table 4**; **Figure 3C**). To better understand TEXH86 and RI-OH temperatures, the mean seasonal and annual temperatures and monthly mean water

TABLE 3 | The contribution of specific GDGTs with depth in core C14.

Sample	Depth (cmbsf)	%isoGDGTs							% (b)	% (OH)		
		% [0]	% [1]	% [2]	% [3]	% [4]	%Cren	%cren'		% [OH-0]	% [OH-1]	% [OH-2]
C10_01	7.5	21.45	5.54	5.82	1.26	12.48	47.67	2.78	2.09	0.25	0.27	0.39
C14_01	37.5	21.68	5.10	5.75	1.21	12.22	47.81	3.16	1.96	0.31	0.33	0.47
C14_02	67.5	20.82	5.45	5.54	1.22	12.00	48.40	3.61	1.93	0.24	0.29	0.50
C14_03	83.75	18.28	9.52	9.78	3.10	3.93	46.79	5.66	2.94	-	-	-
C14_04	97.5	20.79	5.14	5.58	1.20	12.78	48.82	3.13	1.71	0.22	0.25	0.38
C14_05	127.5	20.54	5.14	6.13	1.31	12.46	47.98	3.56	1.87	0.23	0.31	0.47
C14_06	143.75	17.33	7.18	8.69	2.48	8.18	44.51	4.20	7.43	-	-	-
C14_07	157.5	20.96	5.29	5.93	1.26	11.62	48.91	3.41	1.80	0.20	0.27	0.35
C14_08	173.75	25.23	9.14	11.31	1.69	5.60	36.62	4.46	3.33	1.15	0.58	0.89
C14_09	187.5	21.57	5.26	6.07	1.24	11.53	48.52	3.11	1.85	0.20	0.23	0.42
C14_10	203.75	16.29	10.37	12.02	3.03	5.76	36.25	4.91	6.71	1.68	1.19	1.79
C14_11	212.5	20.34	5.45	6.14	1.29	11.86	49.36	3.15	1.57	0.21	0.24	0.39
C14_12	217.5	19.74	5.47	5.55	1.31	11.77	50.44	3.26	1.56	0.22	0.26	0.42
C14_13	228.75	29.09	8.98	9.72	2.30	5.86	33.58	4.74	5.73	-	-	-
C14_14	247.5	20.34	5.31	5.54	1.23	12.97	48.41	3.61	1.76	0.19	0.23	0.41
C14_15	263.75	23.73	9.36	9.82	2.80	4.97	35.58	4.34	5.77	1.74	0.75	1.14
C14_16	277.5	21.19	5.13	5.47	1.18	11.98	49.71	2.95	1.50	0.24	0.25	0.40
C14_17	293.75	27.12	9.35	8.92	2.26	6.14	34.96	5.35	5.90	-	-	-
C14_18	307.5	21.13	5.67	5.65	1.30	12.54	48.32	3.04	1.47	0.24	0.26	0.38
C14_19	323.75	21.95	9.35	10.71	2.11	5.16	34.73	5.66	10.33	-	-	-
C14_20	337.5	19.93	5.24	5.61	1.26	12.36	49.93	3.44	1.42	0.18	0.24	0.39
C14_21	353.75	19.68	9.25	10.39	2.93	6.70	35.68	5.49	5.94	1.80	0.84	1.30
C14_22	367.5	19.90	5.12	5.59	1.17	12.51	50.20	3.22	1.47	0.21	0.25	0.36
C14_23	383.75	18.78	12.18	13.76	3.63	6.19	37.11	5.63	2.72	-	-	-
C14_24	397.5	21.86	5.26	5.80	1.20	12.42	48.27	2.91	1.43	0.23	0.25	0.37
C14_25	413.75	24.83	7.63	9.14	2.24	6.38	37.73	3.98	4.58	1.23	0.94	1.32
C14_26	427.5	22.82	5.83	5.80	1.19	11.66	47.11	2.90	1.62	0.32	0.32	0.43
C14_27	443.75	29.44	7.63	7.50	1.92	4.85	38.14	4.21	3.63	1.24	0.73	0.71
C14_28	457.5	28.62	4.67	3.72	0.86	10.68	46.05	1.90	1.93	0.66	0.53	0.38
C14_29	473.75	23.81	8.90	7.59	1.77	6.13	38.92	2.74	5.37	2.50	1.31	0.96
C14_30	487.5	29.24	4.81	3.62	0.91	11.43	44.48	1.74	2.06	0.73	0.57	0.41
C14_31	503.75	26.67	7.06	6.04	1.46	7.27	40.36	2.16	4.53	2.60	1.10	0.75
C14_32	517.5	29.25	5.17	4.02	0.90	11.48	43.30	1.79	2.18	0.88	0.58	0.45
C14_33	533.75	31.63	6.41	6.54	1.48	8.39	32.20	2.37	5.32	2.32	1.66	1.68
C14_34	547.5	20.13	5.60	5.71	1.14	12.45	49.15	3.09	1.79	0.25	0.31	0.38
C14_35	563.75	23.21	8.50	9.94	2.38	5.47	33.10	5.71	8.29	1.27	1.01	1.12
C14_36	577.5	21.56	5.34	5.96	1.10	12.81	47.57	3.12	1.68	0.25	0.25	0.36

(x), GDGT-x; Cren, crenarchaeol; Cren', crenarchaeol isomer; (b), brGDGTs; (OH-x), OH-GDGT-x

temperatures at different depths are summarized in **Figures 3A,B**.

DISCUSSION

Constrains of GDGT Sources

The isoGDGTs used in TEX_{86} are derived from marine *Thaumarchaeota* (Brochier-Armanet et al., 2008; Spang et al., 2010; Schouten et al., 2013). However, GDGTs-1, -2, -3, and the crenarchaeol isomer can also be synthesized by additional archaea (Sinninghe Damsté et al., 2002; Schouten et al., 2008; Pitcher et al., 2011). For example, marine group II (MG-II) *Euryarchaeota* thriving in shallow water can synthesize GDGTs-1, -2, and -3 (Turich et al., 2007; Schouten et al., 2008). IsoGDGTs from soil and brGDGTs produced *in situ* in marine environments may contribute to the GDGT pool (Hopmans et al., 2004; Peterse et al., 2009; Schouten et al., 2013). Such inputs may affect the application of TEX_{86} in paleotemperature reconstruction. Therefore, indicators such as BIT (Hopmans et al., 2004; De Jonge et al., 2014), GDGT-0/crenarchaeol (Blaga et al., 2009), MI (Zhang et al., 2011), GDGT-2/crenarchaeol (Weijers et al., 2011), %GDGT-2 (Sinninghe Damsté et al., 2012a), and GDGT-2/GDGT-3 (Taylor et al., 2013) were introduced to assess the biological precursors of the isoGDGTs (**Table 1**).

In this study, crenarchaeol was the most abundant component among isoGDGTs, with GDGT-0/crenarchaeol ratios ranging from 0.4 to 1.0 (between 0.2 and 2), suggesting that the isoGDGTs were predominantly produced by MG-I *Thaumarchaeota* in core 14 (Schouten et al., 2008, 2013; Spang et al., 2010). IsoGDGTs introduced by soil and rivers were negligible, as indicated by the low BIT values of 0.01–0.10 (<0.10; **Table 4**; Hopmans et al., 2004; Kim et al., 2010; De Jonge et al., 2014). Apart from terrestrial input, methanotrophic *Euryarchaeota* prevailing in cold seeps can contribute to GDGT-1, -2, and -3 and modify the distribution of isoGDGTs (Elvert et al., 2005; Guan et al., 2019). In this study, the ratios of GDGT-2/crenarchaeol varied from 0.1 to 0.4 (<0.4), GDGT-

TABLE 4 | Various indices were used to evaluate the application of TEX_{86} and reconstruct paleotemperatures in core C14.

Sample	Depth (cmbsf)	Age (kyr)	%GDGT-2	GDGT-0/Cren	GDGT-2/Cren	GDGT-2/GDGT-3	MI	BIT	TEX_{86}^{H}		RI-OH	
									Values	SST (°C)	Values	SST (°C)
C10_01	7.5	0.1	38	0.5	0.1	4.6	0.2	0.02	–0.196	25.2	1.596	24.1
C14_01	37.5	0.7	38	0.5	0.1	4.7	0.2	0.02	–0.177	26.5	1.593	24
C14_02	67.5	0.9	35	0.4	0.1	4.6	0.2	0.01	–0.184	26	1.631	25.4
C14_03	83.75	1.1	35	0.4	0.2	3.2	0.3	0.02	–0.18	26.3	-	-
C14_04	97.5	1.2	37	0.4	0.1	4.7	0.2	0.01	–0.182	26.2	1.605	24.5
C14_05	127.5	1.6	38	0.4	0.1	4.7	0.2	0.02	–0.167	27.2	1.599	24.3
C14_06	143.75	1.8	39	0.4	0.2	3.5	0.3	0.1	–0.166	27.2	-	-
C14_07	157.5	2.0	37	0.4	0.1	4.7	0.2	0.01	–0.176	26.6	1.564	23
C14_08	173.75	2.2	43	0.7	0.3	6.7	0.4	0.06	–0.183	26.1	1.605	24.5
C14_09	187.5	2.3	39	0.4	0.1	4.9	0.2	0.01	–0.177	26.5	1.647	26
C14_10	203.75	2.5	40	0.5	0.3	4.0	0.4	0.05	–0.182	26.2	1.601	24.3
C14_11	212.5	2.6	38	0.4	0.1	4.8	0.2	0.01	–0.18	26.3	1.621	25
C14_12	217.5	2.8	36	0.4	0.1	4.3	0.2	0.01	–0.188	25.8	1.615	24.8
C14_13	228.75	2.9	38	0.9	0.3	4.2	0.4	0.06	–0.186	25.8	-	-
C14_14	247.5	3.1	35	0.4	0.1	4.5	0.2	0.01	–0.179	26.3	1.634	25.5
C14_15	263.75	3.4	37	0.7	0.3	3.5	0.4	0.06	–0.191	25.5	1.601	24.3
C14_16	277.5	3.6	37	0.4	0.1	4.6	0.2	0.01	–0.186	25.9	1.611	24.7
C14_17	293.75	3.9	35	0.8	0.3	4.0	0.3	0.07	–0.195	25.3	-	-
C14_18	307.5	4.1	36	0.4	0.1	4.3	0.2	0.01	–0.195	25.2	1.593	24
C14_19	323.75	4.4	39	0.6	0.3	5.1	0.4	0.1	–0.178	26.4	-	-
C14_20	337.5	4.6	36	0.4	0.1	4.5	0.2	0.01	–0.178	26.4	1.622	25.1
C14_21	353.75	4.9	37	0.6	0.3	3.5	0.4	0.06	–0.174	26.7	1.608	24.6
C14_22	367.5	5.1	37	0.4	0.1	4.8	0.2	0.01	–0.18	26.3	1.59	23.9
C14_23	383.75	5.4	39	0.5	0.4	3.8	0.4	0.03	–0.184	26	-	-
C14_24	397.5	5.6	38	0.5	0.1	4.8	0.2	0.01	–0.185	26	1.591	24
C14_25	413.75	5.9	40	0.7	0.2	4.1	0.3	0.04	–0.175	26.6	1.584	23.7
C14_26	427.5	6.2	37	0.5	0.1	4.9	0.2	0.01	–0.201	24.8	1.575	23.4
C14_27	443.75	6.5	35	0.8	0.2	3.9	0.3	0.03	–0.193	25.4	1.496	20.6
C14_28	457.5	6.7	33	0.6	0.1	4.3	0.2	0.02	–0.236	22.5	1.421	17.9
C14_29	473.75	6.9	36	0.6	0.2	4.3	0.3	0.04	–0.239	22.2	1.424	18
C14_30	487.5	7.0	33	0.7	0.1	4.0	0.2	0.02	–0.247	21.7	1.417	17.7
C14_31	503.75	7.1	36	0.7	0.2	4.1	0.3	0.04	–0.238	22.3	1.406	17.4
C14_32	517.5	7.2	34	0.7	0.1	4.5	0.2	0.02	–0.248	21.6	1.436	18.4
C14_33	533.75	7.4	39	1.0	0.2	4.4	0.3	0.04	–0.209	24.3	1.504	20.9
C14_34	547.5	7.5	37	0.4	0.1	5.0	0.2	0.01	–0.194	25.3	1.548	22.4
C14_35	563.75	7.9	38	0.7	0.3	4.2	0.4	0.08	–0.168	27.1	1.526	21.6
C14_36	577.5	8.2	38	0.5	0.1	5.4	0.2	0.01	–0.183	26.1	1.586	23.8

2/GDGT-3 showed a constant trend below 5.0, the MI index ranged between 0.2 and 0.4 (<0.5), and %GDGT-2 fell in the range of 33–39 (<45), indicating that the contributions of methanotrophic archaea and MG-II *Euryarchaeota* were low (**Table 4**; Blaga et al., 2009; Weijers et al., 2011; Zhang et al., 2011; Sinninghe Damsté et al., 2012a; Taylor et al., 2013). Consequently, isoGDGTs predominantly originating from MG-I *Thaumarchaeota* and TEX_{86}^{H} can be used to reconstruct paleotemperatures in core C14.

Implications of TEX_{86}^{H} Temperatures

TEX_{86}^{H} studies revealed relatively variable temperature records in the OT and ECS (Nakanishi et al., 2012; Xu et al., 2018; Yuan et al., 2018). Yamamoto et al. (2013) compared temperatures derived from Mg/Ca, $U_{37}^{K'}$ and TEX_{86}^{H} at site MD98-2195 of the northern OT. Mg/Ca- and $U_{37}^{K'}$-derived temperatures were assigned to summer and spring seawater temperatures, respectively, because they behaved differently to seasonal variations in the sinking fluxes. Still, the core-top values yielded similarities to summer and spring SSTs, respectively (Yamamoto et al., 2013 and references therein). Since GDGTs in sinking particles were well mixed, the lower TEX_{86}^{H} temperature most likely represented the annual subsurface seawater temperature, as assumed by Yamamoto et al. (2013). However, Zhao et al. (2015) showed similarity between modern summer seawater temperature and core-top TEX_{86}^{H} temperature at the southern OT and concluded that both $U_{37}^{K'}$ and TEX_{86}^{H} temperatures represented summer SSTs. Similar observations were made by Xu et al. (2018), and both $U_{37}^{K'}$ and TEX_{86}^{H} temperatures were used to indicate annual SST at the southern OT. Therefore, TEX_{86}^{H} calibrations for specific locations may be closely related to the specific local hydrology. In this study, the core-top TEX_{86}^{H} and RI-OH temperatures at the study site were 25.2 and 24.1°C, respectively. This is in line with the mean annual SST (24.8°C) and mean annual seawater temperature at 40 m below the sea surface (24.2°C) (**Figure 3A**). In addition, the core-top TEX_{86}^{H} temperature agreed well with the SST in June and November and the average temperature from June to November

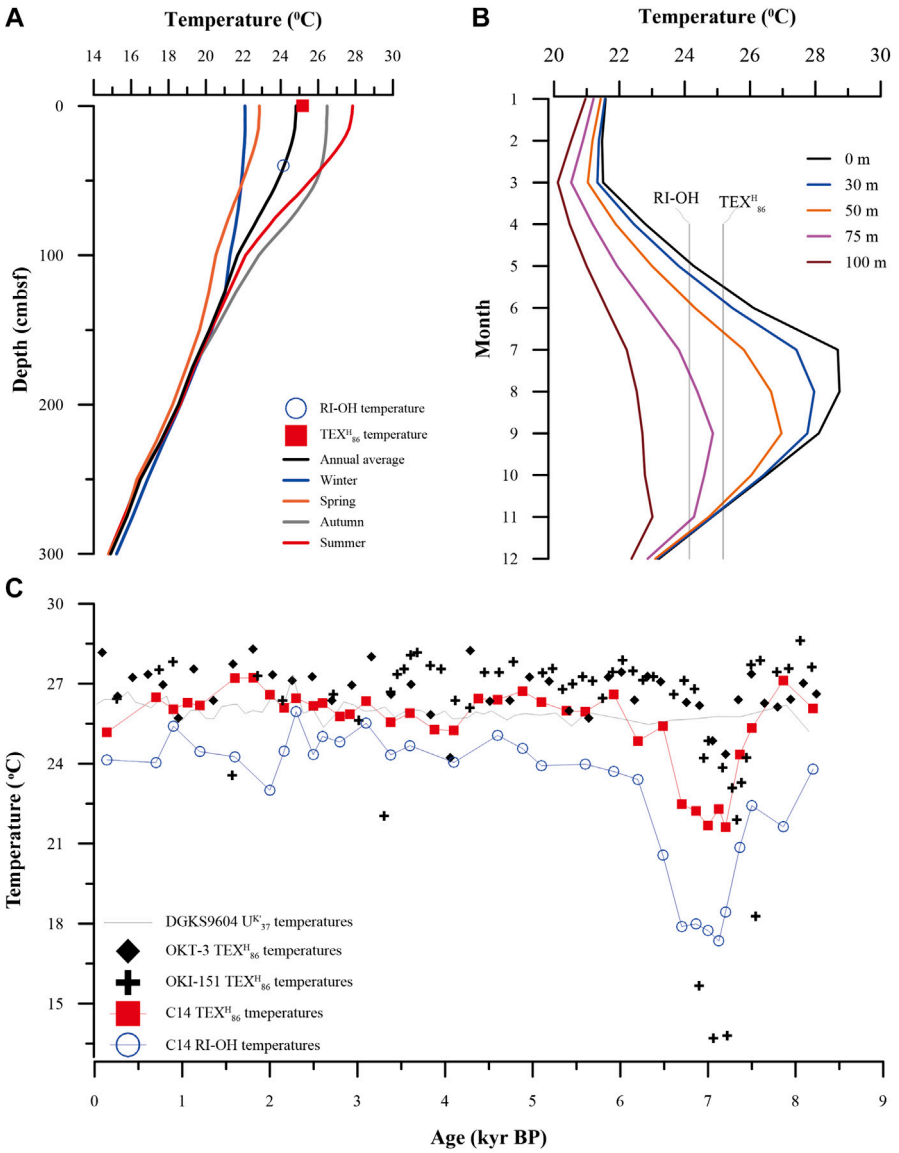

FIGURE 3 | Paleotemperatures derived from core C14 and nearby sites. **(A)** Mean seasonal and annual temperatures at the study site; **(B)** monthly mean water temperatures at different depths at the study site. Data are from Locarnini et al. (2013). **(C)** Comparisons between BIT, TEX_{86}^{H} and RI-OH temperatures from core C14 from the middle OT, TEX_{86}^{H} temperatures from OKT-3 and OKI-151 from the southern OT (Zhao et al., 2015; Xu et al., 2018), and $U_{37}^{K'}$ temperatures from DGKS9604 from the middle OT (Yu et al., 2009).

at depths of 50–7 m (**Figure 3B**). However, TEX_{86}^{H} reflects SST in a specific month, which is unlikely because the GDGTs produced in different seasons have been demonstrated to be suspended and well mixed in the surface water in both the western North Pacific (Yamamoto et al., 2012) and the northern OT (Nakanishi et al., 2012). In this study, the average TEX_{86}^{H} SST (26.1 ± 1°C; except for 7.4–6.6 kyr BP) in core C14 is comparable to the TEX_{86}^{H} SST of the southern OT from 8.2 kyr BP to the present (**Figure 3C**; Zhao et al., 2015; Xu et al., 2018), which is close to the average $U_{37}^{K'}$ SST (26.0 ± 1.3°C; **Figure 3C**) when compared to a nearby site (core DGKS9604; Yu et al., 2009), indicating that the TEX_{86}^{H} temperatures during the last 8.2 kyr BP reflected mean annual SSTs rather than temperatures in a specific short period.

Interestingly, the temperatures derived from RI-OH were generally lower than the TEX_{86}^{H} and $U_{37}^{K'}$ SSTs with a similar changing pattern and trend (**Table 4**; **Figures 3A,C**). To date, the biological precursors of OH-GDGTs remain unclear. To date, OH-GDGTs have been observed in cultures of archaea affiliated with *Thaumarchaeota Group* I.1a (Sinninghe Damsté et al., 2012b; Elling et al., 2014), whereas TEX_{86}-related isoGDGTs are explicitly ascribed to *Thaumarchaeota* Group I.1b (Brochier-Armanet et al., 2008; Spang et al., 2010). The potentially different origins of OH-GDGTs suggest that the RI-OH index may supplement TEX_{86}^{H} in marine environments (Lü et al., 2015). Lü et al. (2015) and Yang et al. (2018) analyzed the surface sediments of the marginal sea in China and revealed a high correlation between RI-OH and the local mean

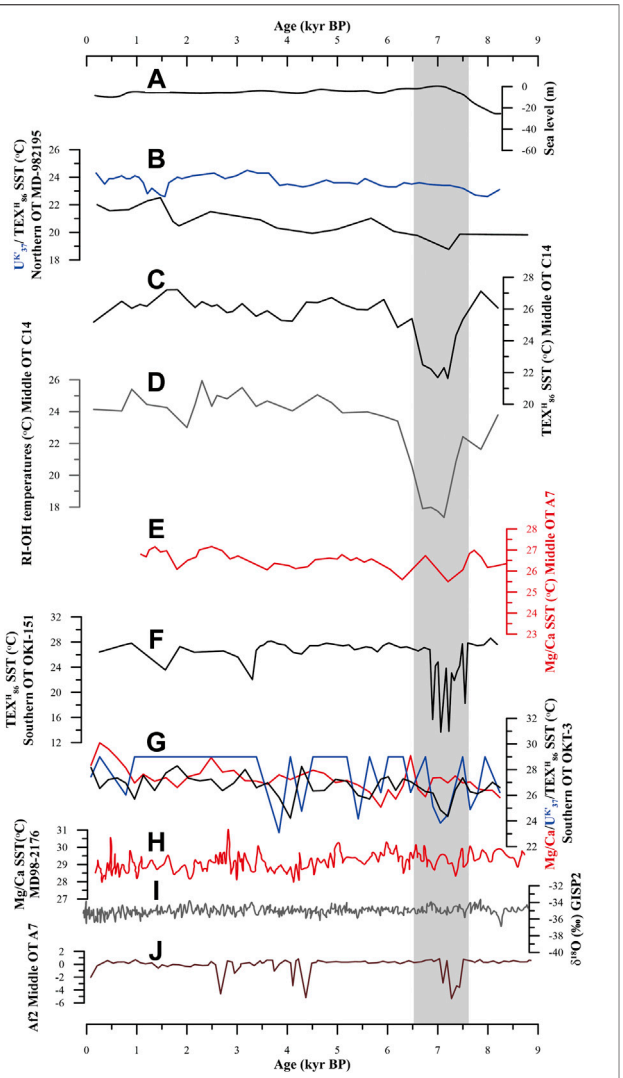

FIGURE 4 | Comparison of paleotemperature variations inferred from core C14 with other paleoclimate data. **(A)** Postglacial sea-level changes in the western Pacific (Liu et al., 2004); **(B)** Temperatures from $U^{K'}_{37}$ (blue) and TEX^{H}_{86} (dark) in core MD98-2195 (Yamamoto et al., 2013); **(C)** TEX^{H}_{86} SST of C14 in this article; **(D)** Temperatures from RI-OH in core C14 in this article; **(E)** Mg/Ca SST of A7 (Sun et al., 2005); **(F)** SST from TEX^{H}_{86} in core OKI-151 (Xu et al., 2018); **(G)** SST from Mg/Ca (red), $U^{K'}_{37}$ (blue) and TEX^{H}_{86} (black) in core OKT-3 (Zhao et al., 2015); **(H)** Mg/Ca SST data from core MD98–2176 in the western tropical Pacific (Stott et al., 2004); **(I)** $\delta^{18}O$ record from the GISP2 ice core (Stuiver and Grootes, 2000); **(J)** the factor representing the western tropical Pacific (Stott et al., 2004); (i) $\delta^{18}O$ record from the GISP2 ice core (Stuiver and Grootes, 2000).

annual SST. Such correlations possibly suggested that OH-GDGTs produced in different seasons have been well mixed in seawater before preservation in sediments (Lü et al., 2015). The core-top RI-OH temperature agreed well with the SSTs in May and December, which most likely reflected subsurface temperatures in the present study (**Figure 3B**).

Cold Events Identified in the Middle Okinawa Trough

In core 14, a warming trend during the last 8.2 kyr BP with an apparent cold event at 7.4–6.6 kyr BP was found using TEX^{H}_{86} and RI-OH proxies. Paleoclimate studies have indicated that the cold anomalies in the North Atlantic may have spread signals of rapid climate changes via the westerlies to the Asian monsoon regions (Dykoski et al., 2005; Sun et al., 2005; Wang et al., 2005). However, studies on the Holocene paleoclimate suggested that the tropical Pacific likely controlled the paleotemperature in East Asia via KC variations rather than the North Atlantic (Lim and Fujiki, 2011; Xu et al., 2018). The KC, the northward branch of the North Pacific subtropical gyre, exerts an influence on the exchange of climatic properties of downstream regions in the Pacific Ocean and is a mediator of the Pacific to the OT (Hu et al., 2015). An intensified trend of the KC since the Holocene has been demonstrated (Sun et al., 2005; Xiang et al., 2007; Diekmann et al., 2008; Yamamoto, 2009). These warm and highly saline waters transported by the KC may have significantly increased the SST of the OT (**Figure 4J**; Zheng et al., 2016). Therefore, the warming of the middle OT may be caused by the enhancement of KC intensities driven by the tropical Pacific during the Holocene. Furthermore, the most remarkable cold event at 7.4–6.6 kyr BP (~7.3 kyr BP) was widely reported in the southern and middle OT (Sun et al., 2005; Zhao et al., 2015; Xu et al., 2018). Since this ~7.3 kyr BP cold event has not been reported in the North Atlantic, factors other than the North Atlantic were likely responsible for the SST decrease in the middle OT (**Figure 4I**; Stuiver and Grootes, 2000). During the 7.4–6.6 kyr BP period, the KC intensity was weakened (Xiang et al., 2007; Hu et al., 2015), potentially contributing to the decreased temperatures of the middle OT (**Figures 4C,J**; Zheng et al., 2016).

However, the ~7.3 kyr BP cold event was magnified in the GDGT-related SST records. In core C14, the TEX^{H}_{86} SST showed a drop of ~5°C at 7.4–6.6 kyr BP (**Figure 4C**). A similar observation has been reported in the southern OT: the TEX^{H}_{86} SST dropped approximately 3–14°C during 7.6–6.9 kyr BP, whereas the Mg/Ca and $U^{K'}_{37}$ SST only showed a drop of 1–3°C during this period (Sun et al., 2005; Kubota et al., 2010; Zhao et al., 2015; Xu et al., 2018). Xu et al. (2018) attributed the 7.6–6.9 kyr BP SST drop to an unknown cold event that occurred during KC intensity weakening. However, the cold event during that period may not be solely responsible for such a large amplitude of decline in TEX^{H}_{86} SST. Global climate change cycles could also have regular influences on the SST of marginal seas (Ho and Laepple, 2015; Ignatov and Gutman, 1999; Debret et al., 2007). Sometimes, the SST of the OT could have suffered from strongly enhanced temperature amplitudes across climate cycles (Debret et al., 2007; Zhao et al., 2014). However, no noticeable long- and short-term climate effect on OT hydrology was reported during the last 7.4–6.6 kyr BP (Bond et al., 1997; Zhao et al., 2014). Factors controlling the abnormal TEX^{H}_{86} SST drop at ~7.3 kyr BP have not been resolved. In core C14, a tephra layer was found from 532.5 to 442.5 cm (K-Ah tephra; 7.4–6.6 kyr BP). A volcanic eruption that occurred at ~7.3 kyr BP has been identified in southwestern Japan (K-Ah tephra; Kitagawa et al., 1995), suggesting that the core C14 site was likely under the scope of the volcanic eruption (**Figure 1**). The K-Ah tephra has been

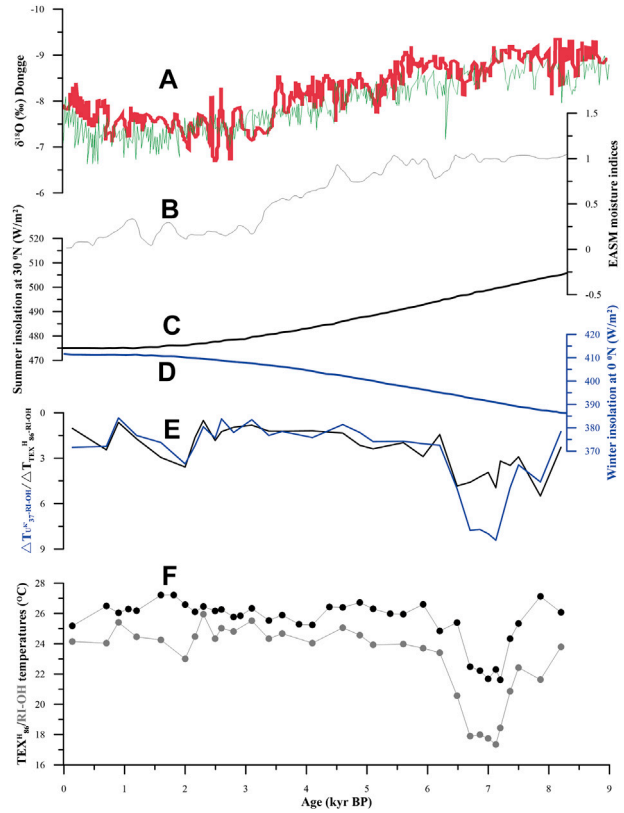

FIGURE 5 | Comparison of sea surface and subsurface temperature differences between TEX_{86}^{H} and RI-OH [$\Delta_{TEX_{86}^{H}-RI-OH}$ (°C)] and between $U_{37}^{K'}$ and RI-OH [$\Delta_{U_{37}^{K'}-RI-OH}$ (°C)] from core C14 ($U_{37}^{K'}$ SST from core DGKS9604 in the study area; Yu et al., 2009) with other paleoclimate data. **(A)** $\delta^{18}O$ records from Dongge Cave stalagmites, China (green: Wang et al., 2005; red: Dykoski et al., 2005); **(B)** the synthesized East Asian summer monsoon (EASM) moisture indices (Wang et al., 2010); **(C)** summer (June) insolation at 30°N (Berger and Loutre, 1991); **(D)** winter (December) insolation at 0°N (Berger and Loutre, 1991); **(E)** $\Delta_{TEX_{86}^{H}-RI-OH}$ (°C) (black) of core C14 and $\Delta_{U_{37}^{K'}-RI-OH}$ (°C) (blue) ($U_{37}^{K'}$ SST from core DGKS9604; Yu et al., 2009); **(F)** temperatures from TEX_{86}^{H} (dark) and RI-OH (gray) in core C14.

widely reported in sediments from the northern to middle OT (Sun et al., 2005; Kubota et al., 2010; Zheng et al., 2016). Modeling studies on Toba volcano in Sumatra have indicated that volcanic eruptions could result in spreading tephra, blocking sunlight, and thus leading to global or regional temperature cooling (Rampino and Self, 1992; Machida, 1999; Oppenheimer, 2002). For core C14, the sedimentation rate during the last 7.4–6.6 kyr BP is exceptionally high (~126 cm/kyr) compared to a nearby site (~20 cm/kyr; DGKS9604; Yu et al., 2009). Therefore, except for the decrease in KC intensity, the cold event and the extremely high sedimentation rate at ~7.3 kyr in core C14 were probably related to volcanic eruptions. The differences between TEX_{86}^{H} SST and SST records from the $U_{37}^{K'}$ and Mg/Ca at ~7.3 kyr BP in the OT may result from distinct sensibilities and responses of specific organisms to climate events (Schouten et al., 2013; Steinke et al., 2008 and references therein). However, the specific and detailed mechanism of the ash impacts on living communities remains unclear and requires further investigation.

Decoupling of the East Asian Summer Monsoon and Paleotemperatures in the Middle OT

The temperature difference between the sea surface and subsurface (ΔT) is sensitive to trace heat and water exchanges, reflecting the depth of the thermocline (DOT) of marginal seas (Jian et al., 2000; Lopes dos Santos et al., 2010; Jia et al., 2012; Yuan et al., 2018). In marginal seas, ΔT has been reported to have a negative relationship with DOT (Jian et al., 2000; Lopes dos Santos et al., 2010; Jia et al., 2012). In the OT, the DOT is mainly controlled by the EAM and KC, which stir the surface of the seawater and cause fluctuations in the DOT. Specifically, the enhancement in the EAM or KC intensities will lead to strengthened mixing of upper water and deepening of the DOT (a reduction in ΔT), and vice versa (Jian et al., 2000; Yamamoto et al., 2013).

In this study, TEX_{86}^{H} and $U_{37}^{K'}$ temperatures (DGKS9604; Yu et al., 2009) were used as SSTs, whereas RI-OH temperatures tentatively served as subsurface temperatures (**Figure 3C**). The temperature differences between TEX_{86}^{H} and RI-OH [$\Delta_{TEX_{86}^{H}-RI-OH}$ (°C)] and between $U_{37}^{K'}$ and RI-OH [$\Delta_{U_{37}^{K'}-RI-OH}$ (°C)] were calculated (**Figure 5E**). From 8.2 kyr BP to the present, a slight overall decrease was found for $\Delta_{TEX_{86}^{H}-RI-OH}$ (°C) and $\Delta_{U_{37}^{K'}-RI-OH}$ (°C), suggesting an increased mixing of the upper water column in the middle OT (**Figure 5E**). Studies on the Holocene EASM intensity showed that the EASM intensity reached a maximum at ~7.0 kyr or ~9.0 kyr (Yang et al., 2019; Liu et al., 2015; Wang et al., 2005; Dykoski et al., 2005). However, the EASM is primarily impacted by summer (June) insolation at 30°N, exhibiting a gradually decreasing trend since 8.2 kyr (**Figure 5C**; Berger and Loutre, 1991). Therefore, the increased mixing of upper water was inconsistent with the EASM intensity, especially over the last 7.0 kyr BP, indicating the decoupling of SSTs in the middle OT with the EASM (**Figures 5A–C**). In the middle Holocene, a decoupling trend between thermal conditions and precipitation has been revealed by pollen sequences from Taiwan (Liew et al., 2006). For land records, decoupling between temperature warming, which was likely caused by the strong influence of low-latitude warm currents, and the EASM intensities were common during the Holocene (Peterse et al., 2011; Park et al., 2014; Wu et al., 2017). The low-latitude warm currents flowing through the OT, such as the KC, may warm and stir the seawater and overstep the influence of high-latitude climates, causing the decoupling of SSTs in the middle OT with the EASM (Zheng et al., 2014, 2016; Xu et al., 2018).

In the present study, the TEX_{86}^{H} SST, revealed a gradual warming trend in the middle OT since 8.2 kyr BP (**Figure 5F**). Modeling of the Holocene climate showed that moderate temperature warming was caused by winter warming that slightly exceeded summer cooling in the tropics (Lorenz et al., 2006). Therefore, the warming trend in the middle OT might be caused by the increased boreal winter insolation at low latitudes (**Figures 5D,F**).

CONCLUSION

Paleotemperatures were reconstructed for the last 8.2 kyr in the middle Okinawa Trough (OT) using TEX_{86}^{H} and RI-OH. IsoGDGTs were mainly derived from marine *Thaumarchaeota,* and TEX_{86}^{H} can be used to reconstruct temperatures of the middle OT, as revealed by GDGT-0/crenarchaeol, BIT, %GDGT-2, and MI. TEX_{86}^{H} temperatures in this study indicated mean annual SSTs close to the $U_{37}^{K'}$ SST of the middle OT. In contrast, RI-OH temperatures were interpreted to represent subsurface temperatures relatively lower than the TEX_{86}^{H} and $U_{37}^{K'}$ SSTs. The cold event at ~7.3 kyr BP and the general warming trend, as revealed by the TEX_{86}^{H} and RI-OH temperatures at 8.2 kyr BP, were attributed to the increasing Kuroshio Current intensity punctuated by a decline at ~7.3 kyr BP. The decreasing temperature differences between TEX_{86}^{H} and RI-OH and between $U_{37}^{K'}$ and RI-OH indicated the decoupling of the SSTs in the middle OT and the East Asian summer monsoon during 8.2 kyr BP. The magnification of the cold phase in TEX_{86}^{H} and the extremely high sedimentation rate at 7.4–6.6 kyr BP were probably partially due to the widespread Kikai-Akahoya tephra (~7.3 kyr).

DATA AVAILABILITY STATEMENT

The original contributions presented in the study are included in the article/**Supplementary Material**, further inquiries can be directed to the corresponding authors.

AUTHOR CONTRIBUTIONS

LL and HG was responsible for writing manuscripts. LX and LL conducted tests. ZS and NW provided the studied samples. HG revised texts, and NW and ZS revised texts and provided comments.

FUNDING

This research was supported by the National Natural Science Foundation of China (91958105 and 91858208) and the Marine S&T Fund of Shandong Province for Pilot National Laboratory for Marine Science and Technology (Qingdao) (No.2021QNLM020002).

ACKNOWLEDGMENTS

The authors are grateful to H. Yang (CUG (Wuhan)] and J. He (GIG, CAS) for technical assistance. We thank F. Xu (CUP, Qingdao) and J. Zhao (QIMG) for offering paleoclimate data, and the help of D. Li (OUC, Qingdao) and X. Lü (CUG (Wuhan)].

SUPPLEMENTARY MATERIAL

The Supplementary Material for this article can be found online at: https://www.frontiersin.org/articles/10.3389/feart.2022.799280/full#supplementary-material

REFERENCES

An, Z., Kutzbach, J. E., Prell, W. L., and Porter, S. C. (2001). Evolution of Asian Monsoons and Phased Uplift of the Himalaya-Tibetan Plateau since Late Miocene Times. *Nature* 411 (6833), 62–66. doi:10.1038/35075035

Berger, A., and Loutre, M. F. (1991). Insolation Values for the Climate of the Last 10 Million Years. *Quat. Sci. Rev.* 10, 297–317. doi:10.1016/0277-3791(91)90033-Q

Blaga, C. I., Reichart, G.-J., Heiri, O., and Sinninghe Damsté, J. S. (2009). Tetraether Membrane Lipid Distributions in Water-Column Particulate Matter and Sediments: a Study of 47 European Lakes along a north-south Transect. *J. Paleolimnol.* 41, 523–540. doi:10.1007/s10933-008-9242-2

Bond, G., Showers, W., Cheseby, M., Lotti, R., Almasi, P., deMenocal, P., et al. (1997). A Pervasive Millennial-Scale Cycle in North Atlantic Holocene and Glacial Climates. *Science* 278, 1257–1266. doi:10.1126/science.278.5341.1257

Brochier-Armanet, C., Boussau, B., Gribaldo, S., and Forterre, P. (2008). Mesophilic Crenarchaeota: Proposal for a Third Archaeal Phylum, the Thaumarchaeota. *Nat. Rev. Microbiol.* 6, 245–252. doi:10.1038/nrmicro1852

De Jonge, C., Hopmans, E. C., Zell, C. I., Kim, J.-H., Schouten, S., and Sinninghe Damsté, J. S. (2014). Occurrence and Abundance of 6-methyl Branched Glycerol Dialkyl Glycerol Tetraethers in Soils: Implications for Palaeoclimate Reconstruction. *Geochimica et Cosmochimica Acta* 141, 97–112. doi:10.1016/j.gca.2014.06.013

Debret, M., Bout-Roumazeilles, V., Grousset, F., Desmet, M., McManus, J. F., Massei, N., et al. (2007). The Origin of the 1500-year Climate Cycles in Holocene North-Atlantic Records. *Clim. Past* 3, 569–575. doi:10.5194/cp-3-569-2007

Diekmann, B., Hofmann, J., Henrich, R., Fütterer, D. K., Röhl, U., and Wei, K.-Y. (2008). Detrital Sediment Supply in the Southern Okinawa Trough and its Relation to Sea-Level and Kuroshio Dynamics during the Late Quaternary. *Mar. Geology.* 255, 83–95. doi:10.1016/j.margeo.2008.08.001

Dykoski, C., Edwards, R., Cheng, H., Yuan, D., Cai, Y., Zhang, M., et al. (2005). A High-Resolution, Absolute-Dated Holocene and Deglacial Asian Monsoon Record from Dongge Cave, China. *Earth Planet. Sci. Lett.* 233, 71–86. doi:10.1016/j.epsl.2005.01.036

Elling, F. J., Könneke, M., Lipp, J. S., Becker, K. W., Gagen, E. J., and Hinrichs, K.-U. (2014). Effects of Growth Phase on the Membrane Lipid Composition of the Thaumarchaeon Nitrosopumilus Maritimus and Their Implications for Archaeal Lipid Distributions in the marine Environment. *Geochimica et Cosmochimica Acta* 141, 579–597. doi:10.1016/j.gca.2014.07.005

Elvert, M., Hopmans, E. C., Treude, T., Boetius, A., and Suess, E. (2005). Spatial Variations of Methanotrophic Consortia at Cold Methane Seeps: Implications from a High-Resolution Molecular and Isotopic Approach. *Geobiology* 3, 195–209. doi:10.1111/j.1472-4669.2005.00051.x

Fietz, S., Huguet, C., Rueda, G., Hambach, B., and Rosell-Melé, A. (2013). Hydroxylated Isoprenoidal GDGTs in the Nordic Seas. *Mar. Chem.* 152, 1–10. doi:10.1016/j.marchem.2013.02.007

Gliozzi, A., Paoli, G., De Rosa, M., and Gambacorta, A. (1983). Effect of Isoprenoid Cyclization on the Transition Temperature of Lipids in Thermophilic Archaebacteria. *Biochim. Biophys. Acta (Bba) - Biomembranes* 735, 234–242. doi:10.1016/0005-2736(83)90298-5

Guan, H., Feng, D., Birgel, D., Peckmann, J., Roberts, H. H., Wu, N., et al. (2019). Lipid Biomarker Patterns Reflect Different Formation Environments of Mussel- and Tubeworm-Dominated Seep Carbonates from the Gulf of Mexico (Atwater Valley and Green Canyon). *Chem. Geology.* 505, 36–47. doi:10.1016/j.chemgeo.2018.12.005

Guo, X., Li, C., Gao, R., Li, S., Xu, X., Lu, Z., et al. (2022). The India-Eurasia Convergence System: Late Oligocene to Early Miocene Passive Roof Thrusting Driven by Deep-rooted Duplex Stacking. *Geosystems and Geoenvironment* 1 (1), 100006. doi:10.1016/j.geogeo.2021.09.005

Ho, S. L., and Laepple, T. (2015). Glacial Cooling as Inferred from marine Temperature Proxies TEX_{86}^{H} and $U_{37}^{K'}$. *Earth Planet. Sci. Lett.* 409, 15–22. doi:10.1016/j.epsl.2014.10.033

Hopmans, E. C., Schouten, S., and Sinninghe Damsté, J. S. (2016). The Effect of Improved Chromatography on GDGT-Based Palaeoproxies. *Org. Geochem.* 93, 1–6. doi:10.1016/j.orggeochem.2015.12.006

Hopmans, E. C., Weijers, J. W. H., Schefuss, E., Herfort, L., Sinninghe Damsté, J. S., and Schouten, S. (2004). A Novel Proxy for Terrestrial Organic Matter in Sediments Based on Branched and Isoprenoid Tetraether Lipids. *Earth Planet. Sci. Lett.* 224, 107–116. doi:10.1016/j.epsl.2004.05.012

Hu, D., Wu, L., Cai, W., Gupta, A. S., Ganachaud, A., Qiu, B., et al. (2015). Pacific Western Boundary Currents and Their Roles in Climate. *Nature* 522, 299–308. doi:10.1038/nature14504

Huang, J., and Sarnthein, M. (2021). One Million Years of Seasonal Seesaw in East Asian Monsoon Winds. *Quat. Sci. Rev.* 274. doi:10.1016/j.quascirev.2021.107277

Huguet, C., Fietz, S., and Rosell-Melé, A. (2013). Global Distribution Patterns of Hydroxy Glycerol Dialkyl Glycerol Tetraethers. *Org. Geochem.* 57, 107–118. doi:10.1016/j.orggeochem.2013.01.010

Huguet, C., Schimmelmann, A., Thunell, R., Lourens, L. J., Sinninghe Damsté, J. S., and Schouten, S. (2007). A Study of the TEX_{86} paleothermometer in the Water Column and Sediments of the Santa Barbara Basin, California. *Paleoceanography* 22, a–n. doi:10.1029/2006PA001310

Ignatov, A., and Gutman, G. (1999). Monthly Mean Diurnal Cycles in Surface Temperatures over Land for Global Climate Studies. *J. Clim.* 12, 1900–1910. doi:10.1175/1520-0442(1999)012<1900:MMDCIS>2.0.CO;2

Ingalls, A. E., Shah, S. R., Hansman, R. L., Aluwihare, L. I., Santos, G. M., Druffel, E. R. M., et al. (2006). Quantifying Archaeal Community Autotrophy in the Mesopelagic Ocean Using Natural Radiocarbon. *Proc. Natl. Acad. Sci.* 103, 6442–6447. doi:10.1073/pnas.0510157103

Jia, G., Zhang, J., Chen, J., Peng, P. a., and Zhang, C. L. (2012). Archaeal Tetraether Lipids Record Subsurface Water Temperature in the South China Sea. *Org. Geochem.* 50, 68–77. doi:10.1016/j.orggeochem.2012.07.002

Jian, Z., Wang, P., Saito, Y., Wang, J., Pflaumann, U., Oba, T., et al. (2000). Holocene Variability of the Kuroshio Current in the Okinawa Trough, Northwestern Pacific Ocean. *Earth Planet. Sci. Lett.* 184, 305–319. doi:10.1016/s0012-821x(00)00321-6

Karner, M. B., DeLong, E. F., and Karl, D. M. (2001). Archaeal Dominance in the Mesopelagic Zone of the Pacific Ocean. *Nature* 409, 507–510. doi:10.1038/35054051

Kim, J.-H., van der Meer, J., Schouten, S., Helmke, P., Willmott, V., Sangiorgi, F., et al. (2010). New Indices and Calibrations Derived from the Distribution of Crenarchaeal Isoprenoid Tetraether Lipids: Implications for Past Sea Surface Temperature Reconstructions. *Geochimica et Cosmochimica Acta* 74, 4639–4654. doi:10.1016/j.gca.2010.05.027

Kitagawa, H., Fukuzawa, H., Nakamura, T., Okamura, M., Takemura, K., Hayashida, A., et al. (1995). AMS 14C Dating of Varved Sediments from Lake Suigetsu, Central Japan and Atmospheric 14C Change during the Late Pleistocene. *Radiocarbon* 37, 371–378. doi:10.1017/S0033822200030848

Kubota, Y., Kimoto, K., Tada, R., Oda, H., Yokoyama, Y., and Matsuzaki, H. (2010). Variations of East Asian Summer Monsoon since the Last Deglaciation Based on Mg/Ca and Oxygen Isotope of Planktic Foraminifera in the Northern East China Sea. *Paleoceanography* 25, a–n. doi:10.1029/2009PA001891

Li, C., Pan, J., and Que, Z. (2011). Variation of the East Asian Monsoon and the Tropospheric Biennial Oscillation. *Chin. Sci. Bull.* 56 (1), 70–75. doi:10.1007/s11434-010-4200-6

Liew, P. M., Lee, C. Y., and Kuo, C. M. (2006). Holocene thermal Optimal and Climate Variability of East Asian Monsoon Inferred from forest Reconstruction of a Subalpine Pollen Sequence, Taiwan. *Earth Planet. Sci. Lett.* 250 (3–4), 596–605. doi:10.1016/j.epsl.2006.08.002

Lim, J., and Fujiki, T. (2011). Vegetation and Climate Variability in East Asia Driven by Low-Latitude Oceanic Forcing during the Middle to Late Holocene. *Quat. Sci. Rev.* 30 (19–20), 2487–2497. doi:10.1016/j.quascirev.2011.05.013

Liu, J., Chen, J., Zhang, X., Li, Y., Rao, Z., and Chen, F. (2015). Holocene East Asian Summer Monsoon Records in Northern China and Their Inconsistency with Chinese Stalagmite $\delta^{18}O$ Records. *Earth-Science Rev.* 148, 194–208. doi:10.1016/j.earscirev.2015.06.004

Liu, J. P., Milliman, J. D., Gao, S., and Cheng, P. (2004). Holocene Development of the Yellow River's Subaqueous delta, North Yellow Sea. *Mar. Geology.* 209, 45–67. doi:10.1016/j.margeo.2004.06.009

Liu, X.-L., Summons, R. E., and Hinrichs, K.-U. (2012). Extending the Known Range of Glycerol Ether Lipids in the Environment: Structural Assignments Based on Tandem Mass Spectral Fragmentation Patterns. *Rapid Commun. Mass. Spectrom.* 26, 2295–2302. doi:10.1002/rcm.6355

Locarnini, R. A., Mishonov, A. V., Antonov, J. I., Boyer, T. P., Garcia, H. E., Baranova, O. K., et al. (2013). World Ocean Atlas 2013, Volume 1: Temperatures. *NOAA Atlas NESDIS* 73, 1–40.

Lopes dos Santos, R. A., Prange, M., Castañeda, I. S., Schefuss, E., Mulitza, S., Schulz, M., et al. (2010). Glacial-interglacial Variability in Atlantic Meridional Overturning Circulation and Thermocline Adjustments in the Tropical North Atlantic. *Earth Planet. Sci. Lett.* 300, 407–414. doi:10.1016/j.epsl.2010.10.030

Lorenz, S. J., Kim, J.-H., Rimbu, N., Schneider, R. R., and Lohmann, G. (2006). Orbitally Driven Insolation Forcing on Holocene Climate Trends: Evidence from Alkenone Data and Climate Modeling. *Paleoceanography* 21 (PA1002), a–n. doi:10.1029/2005pa001152

Lü, X., Liu, X.-L., Elling, F. J., Yang, H., Xie, S., Song, J., et al. (2015). Hydroxylated Isoprenoid GDGTs in Chinese Coastal Seas and Their Potential as a Paleotemperature Proxy for Mid-to-low Latitude Marginal Seas. *Org. Geochem.* 89-90, 31–43. doi:10.1016/j.orggeochem.2015.10.004

Machida, H. (1999). The Stratigraphy, Chronology and Distribution of Distal Marker-Tephras in and Around Japan. *Glob. Planet Change* 21 (1–3), 71–94. doi:10.1016/s0921-8181(99)00008-9

Nakanishi, T., Yamamoto, M., Irino, T., and Tada, R. (2012). Distribution of Glycerol Dialkyl Glycerol Tetraethers, Alkenones and Polyunsaturated Fatty Acids in Suspended Particulate Organic Matter in the East China Sea. *J. Oceanogr.* 68, 959–970. doi:10.1007/s10872-012-0146-4

Oppenheimer, C. (2002). Limited Global Change Due to the Largest Known Quaternary Eruption, Toba ≈74 Kyr BP? *Quat. Sci. Rev.* 21 (14–15), 1593–1609. doi:10.1016/S0277-3791(01)00154-8

Park, J., Lim, H. S., Lim, J., and Park, Y.-H. (2014). High-resolution Multi-Proxy Evidence for Millennial- and Centennial-Scale Climate Oscillations during the Last Deglaciation in Jeju Island, South Korea. *Quat. Sci. Rev.* 105, 112–125. doi:10.1016/j.quascirev.2014.10.003

Peterse, F., Prins, M. A., Beets, C. J., Troelstra, S. R., Zheng, H., Gu, Z., et al. (2011). Decoupled Warming and Monsoon Precipitation in East Asia over the Last Deglaciation. *Earth Planet. Sci. Lett.* 301 (1–2), 256–264. doi:10.1016/j.epsl.2010.11.010

Peterse, F., Schouten, S., van der Meer, J., van der Meer, M. T. J., and Sinninghe Damsté, J. S. (2009). Distribution of Branched Tetraether Lipids in Geothermally Heated Soils: Implications for the MBT/CBT Temperature Proxy. *Org. Geochem.* 40, 201–205. doi:10.1016/j.orggeochem.2008.10.010

Pitcher, A., Hopmans, E. C., Mosier, A. C., Park, S.-J., Rhee, S.-K., Francis, C. A., et al. (2011). Core and Intact Polar Glycerol Dibiphytanyl Glycerol Tetraether Lipids of Ammonia-Oxidizing Archaea Enriched from Marine and Estuarine Sediments. *Appl. Environ. Microbiol.* 77, 3468–3477. doi:10.1128/aem.02758-10

Rampino, M. R., and Self, S. (1992). Volcanic winter and Accelerated Glaciation Following the Toba Super-eruption. *Nature* 359, 50–52. doi:10.1038/359050a0

Reimer, P. J., Bard, E., Bayliss, A., Beck, J. W., Blackwell, P. G., Ramsey, C. B., et al. (2013). Intcal13 and marine13 Radiocarbon Age Calibration Curves 0-50,000 Years Cal BP. *Radiocarbon* 55, 1869–1887. doi:10.2458/azu_js_rc.55.16947

Ruan, J., Xu, Y., Ding, S., Wang, Y., and Zhang, X. (2015). A High Resolution Record of Sea Surface Temperature in Southern Okinawa Trough for the Past 15,000 Years. *Palaeogeogr. Palaeoclimatol. Palaeoecol.* 426, 209–215. doi:10.1016/j.palaeo.2015.03.007

Rueda, G., Rosell-Melé, A., Escala, M., Gyllencreutz, R., and Backman, J. (2009). Comparison of Instrumental and GDGT-Based Estimates of Sea Surface and Air Temperatures from the Skagerrak. *Org. Geochem.* 40, 287–291. doi:10.1016/j.orggeochem.2008.10.012

Schouten, S., Hopmans, E. C., Baas, M., Boumann, H., Standfest, S., Könneke, M., et al. (2008). Intact Membrane Lipids of " Candidatus Nitrosopumilus Maritimus," a Cultivated Representative of the Cosmopolitan Mesophilic Group I Crenarchaeota. *Appl. Environ. Microbiol.* 74, 2433–2440. doi:10.1128/aem.01709-07

Schouten, S., Hopmans, E. C., Schefuß, E., and Sinninghe Damsté, J. S. (2002). Distributional Variations in marine Crenarchaeotal Membrane Lipids: a New Tool for Reconstructing Ancient Sea Water Temperatures? *Earth Planet. Sci. Lett.* 204, 265–274. doi:10.1016/S0012-821X(02)00979-2

Schouten, S., Hopmans, E. C., and Sinninghe Damsté, J. S. (2013). The Organic Geochemistry of Glycerol Dialkyl Glycerol Tetraether Lipids: A Review. *Org. Geochem.* 54, 19–61. doi:10.1016/j.orggeochem.2012.09.006

Sibuet, J.-C., Deffontaines, B., Hsu, S.-K., Thareau, N., Le Formal, J.-P., Liu, C.-S., et al. (1998). Okinawa Trough Backarc basin: Early Tectonic and Magmatic Evolution. *J. Geophys. Res.* 103, 30245–30267. doi:10.1029/98jb01823

Sinninghe Damsté, J. S., Hopmans, E. C., Schouten, S., van Duin, A. C. T., and Geenevasen, J. A. J. (2002). Crenarchaeol: The Characteristic Core Glycerol Dibiphytanyl Glycerol Tetraether Membrane Lipid of Cosmopolitan Pelagic Crenarchaeota. *J. Lipid Res.* 43, 1641–1651. doi:10.1194/jlr.M200148-JLR200

Sinninghe Damsté, J. S., Ossebaar, J., Schouten, S., and Verschuren, D. (2012a). Distribution of Tetraether Lipids in the 25-ka Sedimentary Record of Lake Challa: Extracting Reliable TEX86 and MBT/CBT Palaeotemperatures from an Equatorial African lake. *Quat. Sci. Rev.* 50, 43–54. doi:10.1016/j.quascirev.2012.07.0010.1016/j.quascirev.2012.07.001

Sinninghe Damsté, J. S., Rijpstra, W. I., Hopmans, E. C., Jung, M. Y., Kim, J. G., Rhee, S. K., et al. (2012b). Intact Polar and Core Glycerol Dibiphytanyl Glycerol Tetraether Lipids of Group I.1a and I.1b Thaumarchaeota in Soil. *Appl. Environ. Microbiol.* 78, 6866–6874. doi:10.1128/AEM.01681-12

Spang, A., Hatzenpichler, R., Brochier-Armanet, C., Rattei, T., Tischler, P., Spieck, E., et al. (2010). Distinct Gene Set in Two Different Lineages of Ammonia-Oxidizing Archaea Supports the Phylum Thaumarchaeota. *Trends Microbiol.* 18, 331–340. doi:10.1016/j.tim.2010.06.003

Steinke, S., Kienast, M., Groeneveld, J., Lin, L.-C., Chen, M.-T., and Rendle-Bühring, R. (2008). Proxy Dependence of the Temporal Pattern of Deglacial Warming in the Tropical South China Sea: toward Resolving Seasonality. *Quat. Sci. Rev.* 27, 688–700. doi:10.1016/j.quascirev.2007.12.003

Stott, L., Cannariato, K., Thunell, R., Haug, G. H., Koutavas, A., and Lund, S. (2004). Decline of Surface Temperature and Salinity in the Western Tropical Pacific Ocean in the Holocene Epoch. *Nature* 431 (7004), 56–59. doi:10.1038/nature02903

Stuiver, M., and Grootes, P. M. (2000). GISP2 Oxygen Isotope Ratios. *Quat. Res.* 53, 277–284. doi:10.1006/qres.2000.2127

Sun, Y., Oppo, D. W., Xiang, R., Liu, W., and Gao, S. (2005). Last Deglaciation in the Okinawa Trough: Subtropical Northwest Pacific Link to Northern Hemisphere and Tropical Climate. *Paleoceanography* 20 (4), a–n. doi:10.1029/2004PA001061

Taylor, K. W. R., Huber, M., Hollis, C. J., Hernandez-Sanchez, M. T., and Pancost, R. D. (2013). Re-evaluating Modern and Palaeogene GDGT Distributions: Implications for SST Reconstructions. *Glob. Planet. Change* 108, 158–174. doi:10.1016/j.gloplacha.2013.06.011

Tierney, J. E., and Tingley, M. P. (20142014). A Bayesian, Spatially-Varying Calibration Model for the TEX86 Proxy. *Geochimica et Cosmochimica Acta* 127, 83–106. doi:10.1016/j.gca.2013.11.026

Turich, C., Freeman, K. H., Bruns, M. A., Conte, M., Jones, A. D., and Wakeham, S. G. (2007). Lipids of marine Archaea: Patterns and Provenance in the Water-Column and Sediments. *Geochimica et Cosmochimica Acta* 71, 3272–3291. doi:10.1016/j.gca.2007.04.013

Uda, I., Sugai, A., Itoh, Y. H., and Itoh, T. (2001). Variation in Molecular Species of Polar Lipids from Thermoplasma Acidophilum Depends on Growth Temperature. *Lipids* 36, 103–105. doi:10.1007/s11745-001-0914-2

Wang, Y., Cheng, H., Edwards, R. L., He, Y., Kong, X., An, Z., et al. (2005). The Holocene Asian Monsoon: Links to Solar Changes and North Atlantic Climate. *Science* 308 (5723), 854–857. doi:10.1126/science.1106296

Wang, Y., Liu, X., and Herzschuh, U. (2012). Asynchronous Evolution of the Indian and East Asian Summer Monsoon Indicated by Holocene Moisture Patterns in Monsoonal central Asia. *Quat. Int.* 279-280 (3–4), 526–153. doi:10.1016/j.quaint.2012.08.1829

Weijers, J. W. H., Lim, K. L. H., Aquilina, A., Sinninghe Damsté, J. S., and Pancost, R. D. (2011). Biogeochemical Controls on Glycerol Dialkyl Glycerol Tetraether Lipid Distributions in Sediments Characterized by Diffusive Methane Flux. *Geochem. Geophys. Geosyst.* 12, a–n. doi:10.1029/2011GC003724

Wu, M.-S., Zong, Y., Mok, K.-M., Cheung, K.-M., Xiong, H., and Huang, G. (2017). Holocene Hydrological and Sea Surface Temperature Changes in the Northern Coast of the South China Sea. *J. Asian Earth Sci.* 135, 268–280. doi:10.1016/j.jseaes.2017.01.004

Wu, Z., Li, J., Jin, X., Shang, J., Li, S., and Jin, X. (2014). Distribution, Features, and Influence Factors of the Submarine Topographic Boundaries of the Okinawa Trough. *Sci. China Earth Sci.* 57, 1885–1896. doi:10.1007/s11430-013-4810-3

Xiang, R., Sun, Y., Li, T., Oppo, D. W., Chen, M., and Zheng, F. (2007). Paleoenvironmental Change in the Middle Okinawa Trough since the Last Deglaciation: Evidence from the Sedimentation Rate and Planktonic Foraminiferal Record. *Palaeogeogr. Palaeoclimatol. Palaeoecol.* 243, 378–393. doi:10.1016/j.palaeo.2006.08.016

Xu, F., Dou, Y., Li, J., Cai, F., Zhao, J., Wen, Z., et al. (2018). Low-latitude Climate Control on Sea-Surface Temperatures Recorded in the Southern Okinawa Trough during the Last 13.3 Kyr. *Palaeogeogr. Palaeoclimatol. Palaeoecol.* 490, 210–217. doi:10.1016/j.palaeo.2017.10.034

Xu, L. F., Guan, H. X., Sun, Z. L., Wang, L. B., Mao, S. Y., Liu, L. H., et al. (2020). The Response Mechanism of Organic Matters and Paleoenvironmental Changes in the central Okinawa Trough during the Last 8.2 Ka. *Geochimica (Chinese)* 6, 653–665.

Yamamoto, M., Kishizaki, M., Oba, T., and Kawahata, H. (2013). Intense winter Cooling of the Surface Water in the Northern Okinawa Trough during the Last Glacial Period. *J. Asian Earth Sci.* 69, 86–92. doi:10.1016/j.jseaes.2012.06.011

Yamamoto, M. (2009). Response of Mid-latitude North Pacific Surface Temperatures to Orbital Forcing and Linkage to the East Asian Summer Monsoon and Tropical Ocean-Atmosphere Interactions. *J. Quat. Sci.* 24, 836–847. doi:10.1002/jqs.1255

Yamamoto, M., Shimamoto, A., Fukuhara, T., Tanaka, Y., and Ishizaka, J. (2012). Glycerol Dialkyl Glycerol Tetraethers and TEX86 index in Sinking Particles in the Western North Pacific. *Org. Geochem.* 53, 52–62. doi:10.1016/j.orggeochem.2012.04.010

Yang, X., Yang, H., Wang, B., Huang, L.-J., Shen, C.-C., Edwards, R. L., et al. (2019). Early-Holocene Monsoon Instability and Climatic Optimum Recorded by Chinese Stalagmites. *The Holocene* 29, 1059–1067. doi:10.1177/0959683619831433

Yang, Y., Gao, C., Dang, X., Ruan, X., Lü, X., Xie, S., et al. (2018). Assessing Hydroxylated Isoprenoid GDGTs as a Paleothermometer for the Tropical South China Sea. *Org. Geochem.* 115, 156–165. doi:10.1016/j.orggeochem.2017.10.014

Yu, H., Liu, Z., Berné, S., Jia, G., Xiong, Y., Dickens, G. R., et al. (2009). Variations in Temperature and Salinity of the Surface Water above the Middle Okinawa Trough during the Past 37kyr. *Palaeogeogr. Palaeoclimatol. Palaeoecol.* 281, 154–164. doi:10.1016/j.palaeo.2009.08.002

Yuan, Z., Xiao, X., Wang, F., Xing, l., Wang, Z., Zhang, H., et al. (2018). Spatiotemporal Temperature Variations in the East China Sea Shelf during the Holocene in Response to Surface Circulation Evolution. *Quat. Int.* 482, 46–55. doi:10.1016/j.quaint.2018.04.025

Zhang, Y. G., and Liu, X. (2018). Export Depth of the TEX 86 Signal. *Paleoceanography and Paleoclimatology* 33, 666–671. doi:10.1029/2018PA003337

Zhang, Y. G., Zhang, C. L., Liu, X.-L., Li, L., Hinrichs, K.-U., and Noakes, J. E. (2011). Methane Index: A Tetraether Archaeal Lipid Biomarker Indicator for Detecting the Instability of marine Gas Hydrates. *Earth Planet. Sci. Lett.* 307, 525–534. doi:10.1016/j.epsl.2011.05.031

Zhao, J., Li, J., Cai, F., Wei, H., Hu, B., Dou, Y., et al. (2015). Sea Surface Temperature Variation during the Last Deglaciation in the Southern Okinawa Trough: Modulation of High Latitude Teleconnections and the Kuroshio Current. *Prog. Oceanography* 138, 238–248. doi:10.1016/j.pocean.2015.06.008

Zhao, M., Ding, L., Xing, L., Qiao, S., and Yang, Z. (2014). Major Mid-late Holocene Cooling in the East China Sea Revealed by an Alkenone Sea Surface Temperature Record. *J. Ocean Univ. China* 13, 935–940. doi:10.1007/s11802-014-2641-2

Zheng, X., Li, A., Kao, S., Gong, X., Frank, M., Kuhn, G., et al. (2016). Synchronicity of Kuroshio Current and Climate System Variability since the Last Glacial Maximum. *Earth Planet. Sci. Lett.* 452, 247–257. doi:10.1016/j.epsl.2016.07.028

Zheng, X., Li, A., Wan, S., Jiang, F., Kao, S. J., and Johnson, C. (2014). ITCZ and ENSO Pacing on East Asian winter Monsoon Variation during the Holocene: Sedimentological Evidence from the Okinawa Trough. *J. Geophys. Res. Oceans* 119, 4410–4429. doi:10.1002/2013JC009603

Conflict of Interest: The authors declare that the research was conducted in the absence of any commercial or financial relationships that could be construed as a potential conflict of interest.

Publisher's Note: All claims expressed in this article are solely those of the authors and do not necessarily represent those of their affiliated organizations, or those of the publisher, the editors and the reviewers. Any product that may be evaluated in this article, or claim that may be made by its manufacturer, is not guaranteed or endorsed by the publisher.